www.czasopisma.pan.pl PAN POLSKA AKADEMIA NAUK www.journals.pan.pl

A R C H I V E S O F M E T A L L U R G Y A N D M A T E R I A L S

Volume 60 2015 Issue 3

DOI: 10.1515/amm-2015-0378

M. KOT*#

DEFORMATION AND FRACTURE ANALYSIS OF COATING-SUBSTRATE SYSTEMS

ANALIZA ODKSZTAŁCENIA I PĘKANIA W UKŁADZIE POWŁOKA-PODŁOŻE

The paper presents the deformation and fracture analysis of coating-substrate systems during spherical indentation. CrN and TiN ceramic coatings with a thickness of 1-5 μm were tested using 10 to 200 μm tip radius spherical indenters. The typical results of indentation tests i.e. force-penetration depth curves were transformed into stress-strain curves using an algorithm developed by the author. The test results are compared with the results of numerical analysis conducted using FEM modelling. Such a complex analysis allows users to determine the level of tensile stress leading to the formation of cracks observed using SEM and TEM microscopy, and to define the failure maps for the coating substrate-systems.

Keywords: coatings, deformation, stress, fracture

W pracy przedstawiono analizę deformacji i pękania układów powłoka-podłoże przy użyciu testów indentacji i sferycznych wgłębników. Badano powłoki CrN i TiN o grubościach z zakresu 1-5 μm stosując wgłębniki o promieniach zaokrąglenia z zakresu 10 do 200 μm. Typowe wyniki testów w postaci krzywych siła-głębokość penetracji transformowano na krzywe naprężenie-odkształcenie przy użyciu algorytmu opracowanego przez autora. Wyniki porównywano z wynikami modelowania przy użyciu metody elementów skończonych MES. Taka procedura pozwoliła określić stan naprężeń rozciągających prowadzących do powstawania pęknięć obserwowanych przy użyciu mikroskopii skaningowej SEM i transmisyjnej TEM. Opracowano także mapy deformacji badanych układów powłoka-podłoże.

1. Introduction

Thin, hard surface layers and coatings are increasingly used in mechanical engineering, mainly in order to reduce wear and minimize friction. Many of the coatings are deposited by PVD and CVD techniques, and typical materials are carbides or nitrides of transition metals or carbon with different sp^2 to sp^3 bonds ratio. Ceramic coatings are characterized by high hardness, high elasticity modulus and in many cases, high wear and corrosion resistance. The great interest in carbon coatings derives from their excellent tribological properties. Their low coefficients of friction in contact with a number of engineering materials is primarily a result of the formation of a thin graphite tribolayer on the surface, which significantly reduces friction [1]. However, the main problem of both these groups of coatings is their low fracture resistance, limiting their application especially under dynamic or impact loading. The value of their fracture toughness K_{IC} = 1-10 MPa · $m^{1/2}$ is tens of times lower than for metal alloys. Their fracture resistance can be improved by modifying the architecture and microstructure, as is the case for multilayers [2,3], and nanocomposite coatings [4,5], characterized by significantly better mechanical properties over single coatings. Multilayer coatings can consist of various types of materials, while for machine parts mainly ceramic/metal ones, such as Ti / TiN [6] and Cr/CrN [2,7], are proposed. The hard ceramic layers are responsible for the tribological properties and metal layers reduce stress and improve adhesion to the substrate. Microscopic examination showed that such multilayer coatings exhibited improved fracture resistance than single ceramic coatings. This is due to the interaction between the layers that leads to the specific failure mechanism. Microcracks appear on the surface of the ceramic layers and propagate through their whole thickness towards the interface with soft layers, where they are stopped in locally yielded metal layers [8]. Crack initiation in the

* AGH UNIVERSITY OF SCIENCE AND TECHNOLOGY, FACULTY OF MECHANICAL ENGINEERING AND ROBOTICS, AL. A.MICKIEWICZA 30, 30-059 KRAKOW, POLAND

Corresponding author: kotmarc@agh.edu.pl

next ceramic layer when stress reaches a critical level requires a rise in load. The total effect of fracture toughness enhancement of a ceramic/metal multilayer could be significant considering that these metal layers may number even several dozen. A similar effect was also observed for the multilayers with hydrogenated carbon and thin titanium layers TiN / Ti / a-C:H [9]. However, in the nanocomposite coatings, such a barrier to easy crack propagation in a usually amorphous a-C:H, a-C, a-Si_3N_4 matrix are carbides or nitride nanoparticles WC, CrC, TiN [5,10,11]. The optimization of nanocomposite microstructure was presented in a previous paper [4]. However, even the best coating will not fulfil its functions if the substrate does not provide adequate support. The large contact stresses, being a result of external loads, can lead to local plastic deformation of the substrate. The development of a plastically deformed zone is responsible for the large deformation of the whole coating-substrate system and, in the case of stiff and low fracture resistant coatings, for their fracture, chipping and premature wear [12]. To prevent this phenomenon, additional treatments are applied for substrate strengthening i.e. nitriding or hardening [13,14] and for surfaces with further coating deposition these technologies are called duplex. Unfortunately, despite the rapid development of deposition technology and design of the newest groups of sophisticated coatings, the problem of the coating selection to specific applications has still not been solved. This is due to the lack of mathematical equations for determining the load bearing capacity of coated surfaces. For homogeneous materials, engineers use the Hertz theory [15,16], which allows them to calculate the stress field, deformation and predict the yield strength when load and contact geometry are known. However, there are many assumptions in this theory that preclude it for the coating-substrate systems where the coating has different properties than the core material. In addition, local plastic deformation may occur in metal substrates at high contact loads. There are some studies where the authors developed Hertz equations for coated components [17]. Their essence is the introduction of additional correction factors that depend on the contact geometry, coating and substrate properties and coating thickness to well known equations valid for homogeneous materials.

The mechanical testing of coating-substrate systems is very commonly conducted using an instrumental indentation method, where load and penetration depth are continuously measured while pressing an indenter with a defined geometry into the surface. The obtained indentation load-penetration depth curves allow users to calculate the hardness and elasticity modulus of the tested samples [18]. The obtained results correspond to coating properties at small deformations and loads usually in a range of several milinewtons.

But still the problem is how to determine the fracture toughness of coatings, therefore this parameter for brittle coatings is extremely important. In the literature, there are some techniques for determination of a coating's fracture resistance, like three-point bending [19], buckling [20], and uniaxial stretching [21]. Each of them has its own limitations, but the techniques most often used for calculating the K_{IC} parameter are indentation and scratch tests. Many equations are given for K_{IC} determined from indentation experiments but all of them link material properties, load and length of cracks on the coating surface. Analysis of indentation curves makes it possible to determine the amount of energy dissipated during the crack formation U, which can be seen in the curves as a sudden increase in penetration depth called pop-in. Li et al [22] proposed the relation for fracture toughness K_{IC} of thin films as:

$$K_{IC} = \left[\left(\frac{E}{\left(1-\nu^2\right)2\pi C_R}\right)\left(\frac{U}{t}\right)\right]^{1/2} \tag{1}$$

where E is Young's modulus, ν – Poisson number, $2\pi CR$ crack length and t is a coating thickness.

However, for thin coatings, it is difficult to exclude the influence of the substrate on the measurement results because the deformation of the system to some extent are restricted by the substrate and the cracked coating is still supported on the substrate. On the other hand, from the designer's point of view, it is necessary to know how the whole system, not the coating itself, deformations are acceptable and what the load is at which a specific form of the coating-substrate system destruction appears. In the face of many problems encountered in the construction of analytical models for the analysis of deformation and stress distribution in coating-substrate systems, the numerical method based on finite element modelling (FEM) is a very effective and commonly used tool. Most frequently indentations of coatings deposited on elastic or elastic-plastic substrates [23,24], and even coatings with a complex structure as multilayers [25,26] are modelled. The aim of these studies is to find the critical loads leading to the plastic deformation of the substrate, coating fracture or delamination.

The author of the paper proposes to analyse the deformation of coating-substrate systems method based on complex analysis of indentation curves, their transformation into stress-strain σ curves and comparison with modelling results (algorithm in Fig. 1). These $\sigma - \varepsilon$ curves are plotted by measuring the contact radius a_C corresponding to the actual load F and calculated from the following equations [27]:

$$\sigma = p_m = \frac{F}{\pi \cdot a_C^2}, \quad \varepsilon_i = \frac{0,2a_c}{R_i}, \quad a_C = \sqrt{2h_C R_i - h_C^2} \tag{2}$$

where: R_i – indenter tip radius, h_C – contact depth.

Comparing the mean pressure, stress distribution and concentration areas, the maximum tensile stress level leading to brittle failure of the coating can be determined. It should be noted that residual stresses, usually compressive in PVD deposition processes for ceramic and carbon coatings (up to a few GPa [28,29]), must be added to the stress field derived from external loading. The presented procedure for analysing the mechanical properties of coated surfaces, including analysis of the experimental and modelling results, allows to create failure maps for the coating-substrate systems, and can be helpful in the selection of the coating and its thickness optimal for a particular application. To break free from a particular contact geometry, such maps are created in the relative thickness t/R_i (t – thickness

of the coating, R_i – the radius of the indenter) and the relative load F/R_i^2 (F – critical load leading to the characteristic forms of destruction) coordinates.

2. Experimental part

TiN and CrN coatings were deposited by unbalanced DC pulsed magnetron sputtering. Prior to deposition, 25×25×1 mm X10CrNi18-8 austenitic steel substrates were cleaned in an industrial washing machine (Miele, Guetersloh, Germany) with tenside washing agents, dried and mounted on a 3D rotable planetary in the industrial-like R&D deposition equipment (Leybold Vakuum, Cologne, Germany). After pumping to high vacuum conditions (2×10^{-5} mbar), ion plasma treatment was performed without prior heating of the chamber and substrates at room temperature. Titanium nitride and chromium nitride were deposited using pure titanium and chromium targets (RHP Technologies, Seibersdorf, Austria) in an Ar-N_2 gas flow. A suitable thickness of the coatings was obtained by changing the time of deposition, while the growth rate was previously found for thicker coatings. CrN coatings 1 and 5.2 µm and TiN 1 and 2.4 µm thick were tested by instrumented indentation techniques to analyse the deformation and fracture of coating-substrate systems. Tests were conducted with different spherical indenter radii R_i = 10, 20, 50 and 200 µm. These indenters allowed users to obtain the various states of deformation and stress distribution, dependent mainly on the relative film thickness t/R_i as shown in previous works [12,27]. Within the analysed indenters and coating thickness, this parameter varied inside the range $0.005 \leq t/R_i \leq 0.5$. Indentation curves were analysed using the algorithm shown in Figure 1 and described above.

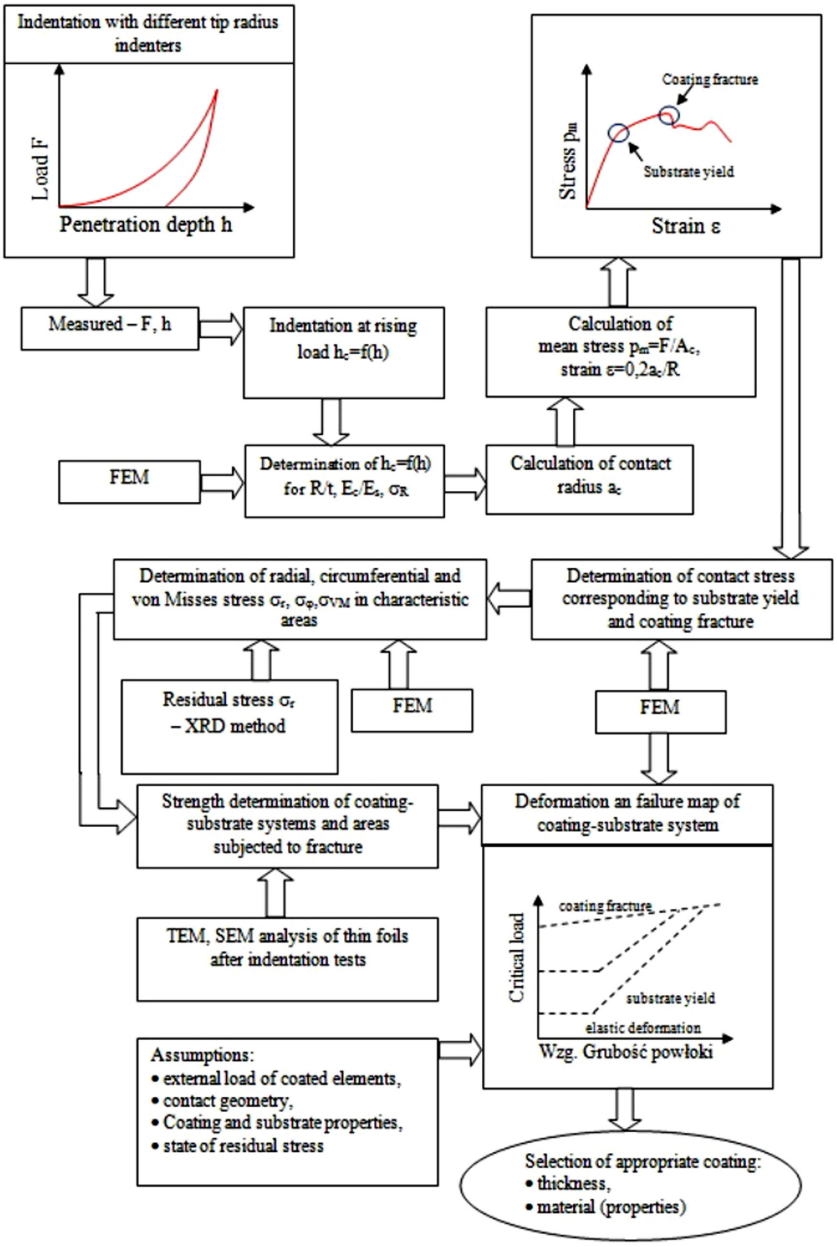

Fig. 1. Diagram of a complex analysis of spherical indentation using the experiment and FEM modelling results

Numerical experiments were also conducted using FEM and the ANSYS 15 software. A 2D axisymmetric model of the coating-substrate system and indenter with a fixed finite element mesh is shown in Figure 2.

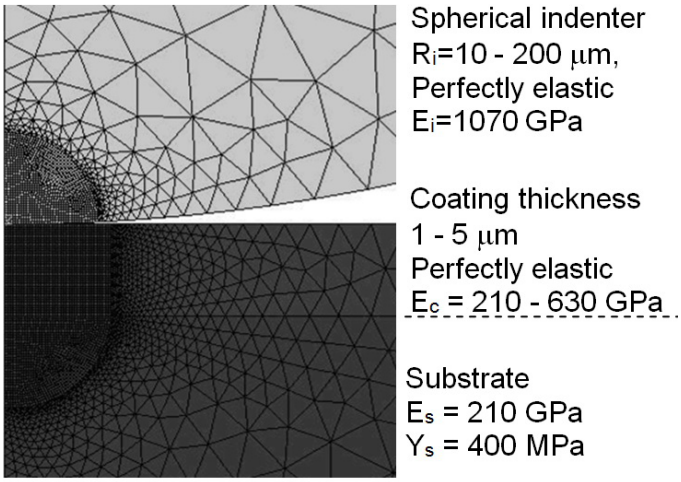

Fig. 2. Part of finite element model of indenter pressed into coated substrate, with the refined meshes in the region around contact zone

The boundary conditions were specified so that the model matches the real indentation experiments on the coating-substrate system. Nodes in the bottom plane of the model were fixed assuming the deformation u_y and $u_z = 0$, while nodes on the symmetry axis of the indenter (left side) cannot move in the radial direction $u_y = 0$. The size of the model means that the elastic deformation in the substrate did not reach the bottom and right plane of the model, hence it may be considered as infinitely large. Both dimensions of the model were over 40 times higher than the maximal radius of the contact area. A very fine mesh, an 8-node element "solid structural 2D PLANE183" [30] with additional nodes on the sides of the element, were used in the coating and the substrate near the contact zone for accurate analysis of strain and stress fields where the stress concentration was expected (Fig. 2). Even the thinnest coating had 10 nodes in the z-direction, while for thicker coatings the number of nodes was higher. Normal load was gradually applied on the top of the indenter with at least 50 steps during loading and unloading up to a maximum selected value and down to zero. FEM analysis was conducted to determine the effect of the contact geometry and material properties on:

- stress distributions at different ranges of coating-substrate system deformation,
- areas subjected to maximum radial stress concentration leading to coating fracture.

3. FEM modelling results

The action of the indenter on a coating-substrate system is different for thin and thick coatings. Thick coatings substantially reduce the deformations of the whole system, as is shown in the indentation curves for 1 and 5 μm thick coatings and a 20 μm indenter tip radius (Fig. 3).

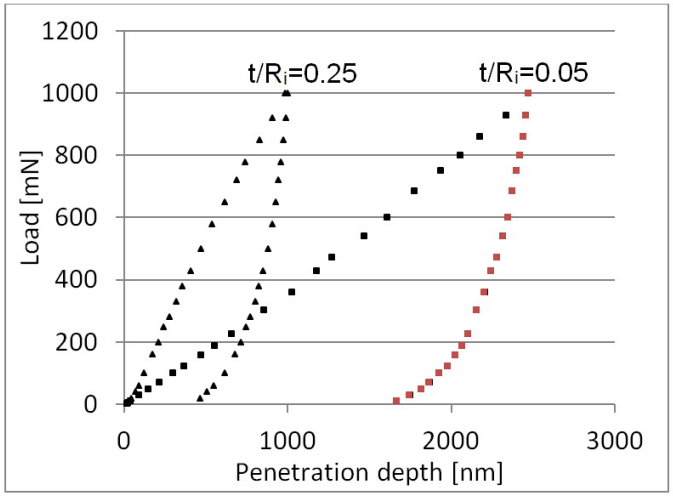

Fig. 3. Modelled indentation curves of coating-substrate systems with different t/R_i ratio

For a 1 μm coating ($t/R_i = 0.05$) the maximum penetration depth is 2450 nm, while for 5 μm ($t/R_i = 0.25$) it is reduced to 1000 nm. In comparison, the penetration depth for an uncoated substrate is 2700 nm. Initially, in the elastic state of deformation, the radial stresses depend mainly on the elasticity modulus of the coatings. The rise in coating stiffness results in a smaller contact radius and contact area between the coating and indenter and hence higher contact pressure. Figure 4a shows the change in radial stress on the coating surface at a 1 mN load. An increase in the coating elasticity modulus E_c also leads to an increase in maximum tensile stress at the surface of the coating from 280 to 440 MPa for E_c = 210 and 630 GPa, respectively. At small loads the increase in coating thickness from 1 to 5 μm does not greatly affect the stress distribution in the contact area (Fig. 4b). Meanwhile tensile stress grows from 340 to 410 MPa (detail Fig. 4b).

Significant differences in the contact mechanics of coating-substrate systems appear at higher loads when the substrate is locally plastically deformed below the contact zone [31]. The analyses presented in the previous work have shown that the substrate yield occurred at F_{PL} load [27]:

$$\frac{F_{Pl}}{R_i^2} = A \cdot Y_S \cdot \left(\frac{E_C}{E_S} + B\right)\left(\frac{t}{R_i}\right)^2 + 21{,}08 \cdot \frac{Y_S^3}{E_{ind}^2} \tag{3}$$

where: Y_S – substrate yield strength, R_i – indenter radius, E – elasticity modulus, A and B – coefficients determined from the FEM modelling. Meanwhile, the reduced elasticity modulus E_{ind} is calculated from the equation $E_{ind} = \dfrac{1}{\dfrac{1-\nu_D^2}{E_D} + \dfrac{1-\nu_S^2}{E_S}}$. The subscripts c, s and d denote coating, substrate and diamond indenter. For an uncoated substrate the yield can be predicted from the equation which is the second part of the sum in equation (3):

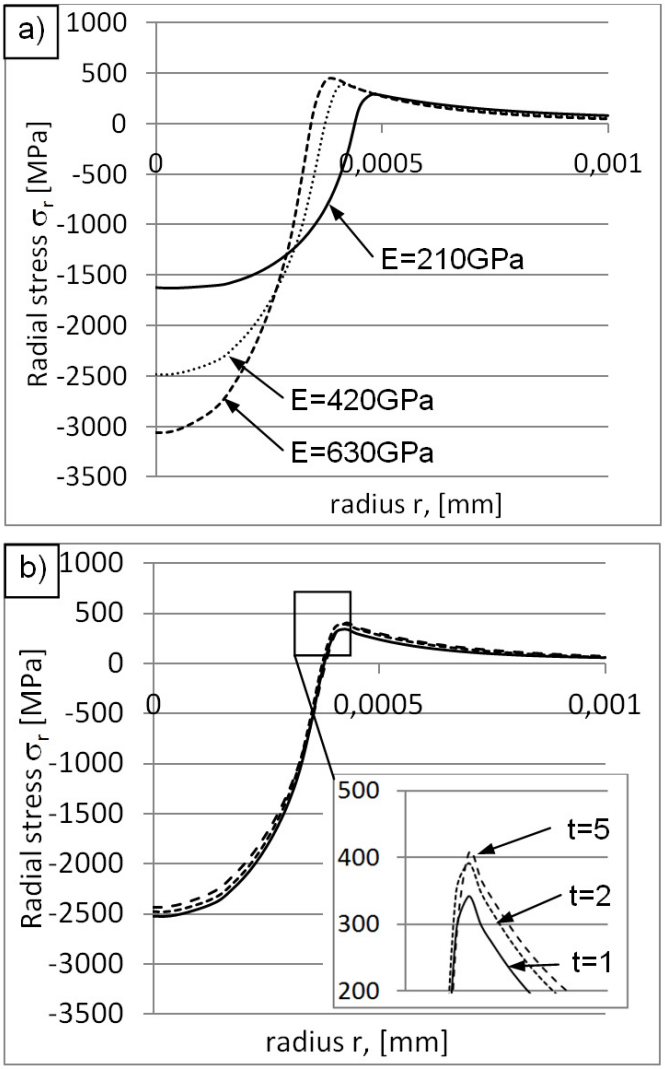

Fig. 4. Radial stress distributions in elastic deformation regime for: a) 2 μm coatings with different elasticity modulus, b) coatings E = 420GPa with different thickness t

$$\frac{F_{pl}}{R_i^2} = 21{,}08 \cdot \frac{Y_S^3}{E_{ind}^2} \tag{4}$$

The values of the A and B coefficients vary from 0.85 to 1.1 and from 0.5 to 1.2 respectively [27]. Higher values correspond to smaller values of Ec/Es (the ratio of the coating and substrate elasticity modulus) and higher yield strength. Initially, for $t/R_i < 0.01$ coatings, it does not increase the load bearing capacity of the surface. FEM results indicate that the stress distribution in the system with such a thin coating is practically the same as for the uncoated substrate. Above this relative thickness, the coating starts to play a greater role and the substrate no longer has to carry the whole load. For all the analysed coating-substrate systems, substrate yield occurred at h_{max}/t = 0.004-0.04. Equation (3) indicates that F_{pl} increases with the square of coating thickness. The plastic deformation of metallic substrates at higher loads leads to the formation of pile-up around the contact area. This pile-up is greater for lower relative coating thickness t/R_i. In Figure 5 there is a large pile-up for the thick coating t/R_i = 1/20, and its lack for the thin coating t/R_i = 1/200 at the 1N load.

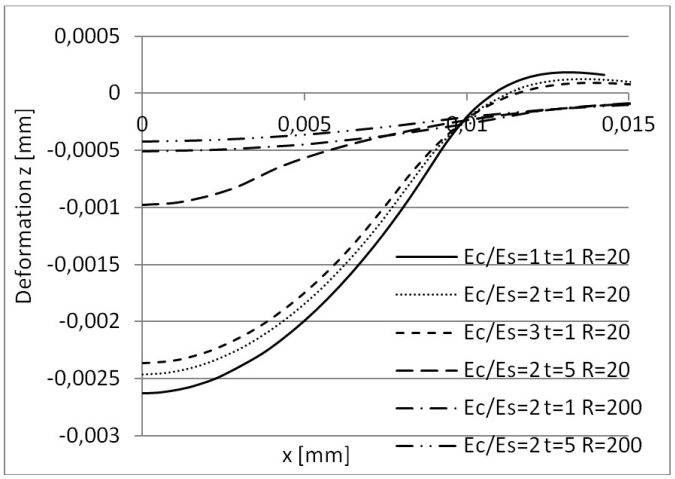

Fig. 5. The surface of the coating-substrate systems profiles under 1N load

This large substrate deformation induces high tensile stresses at the surface and above the coating strength to its fracture.

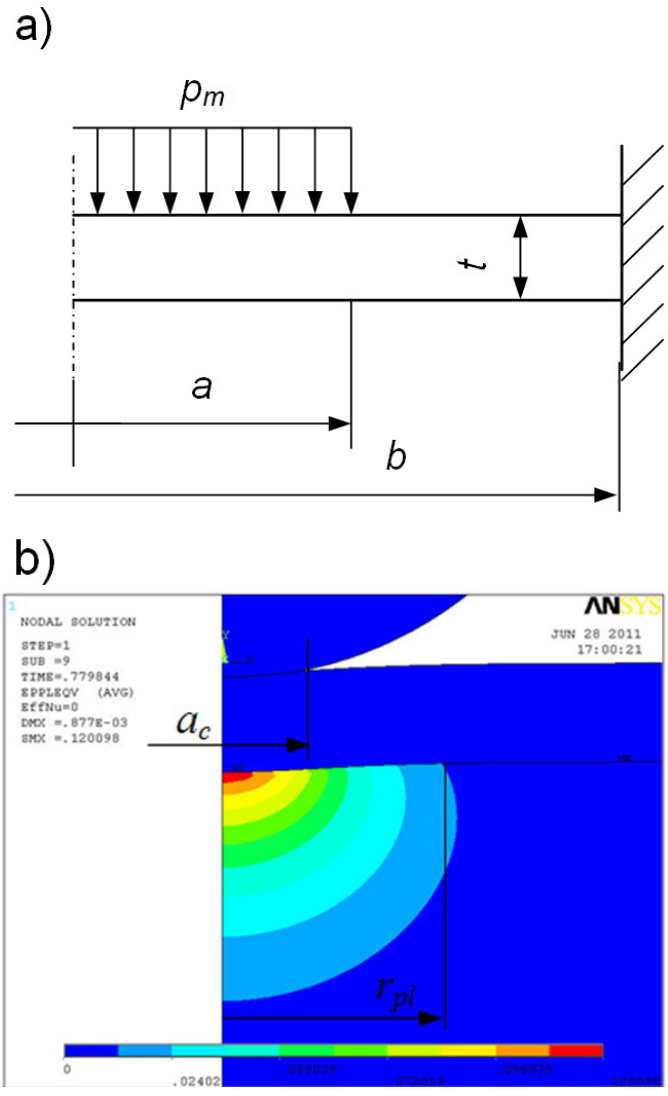

Fig. 6. Analogy of the coating-substrate system deformation b), to the deformation of circular plate with constant load acting on fixed radius a).

The stress maxima correspond to the minima of radius at which the coating is bent. From a mechanical point of view, the stress state is similar to the deformation of the circular plate fixed at its ends – radius b and loaded by p_m pressure in the radius a (Fig. 6a). Stress on the upper and lower surface of the plate can be calculated as:

$$\sigma_R(bottom) = \frac{3 \cdot p_m \cdot a_c^2}{4 \cdot t^2}\left[(1+\nu_c)\cdot(2ln\frac{r_{pl}}{a_c}+\left(\frac{a_c}{r_{pl}}\right)^2 - 1\right]$$

$$\sigma_R(top) = \frac{3 \cdot p_m \cdot a_c^2}{2 \cdot t^2}\left(\frac{a_c}{t}\right)^2\left[1-\left(\frac{a_c}{r_{pl}}\right)^2\right] \quad (5)$$

For the coating-substrate system it can be assumed (Fig. 6b) that b corresponds to the radius of the plastically deformed zone in the substrate r_{pl} and a corresponds to the radius of the contact zone a_c. The larger stress is mainly determined by the a_c/t and a_c/r_{pl} ratios. The radial stress distribution at a 1 N load is quite different for thin and thick coatings (Fig. 7).

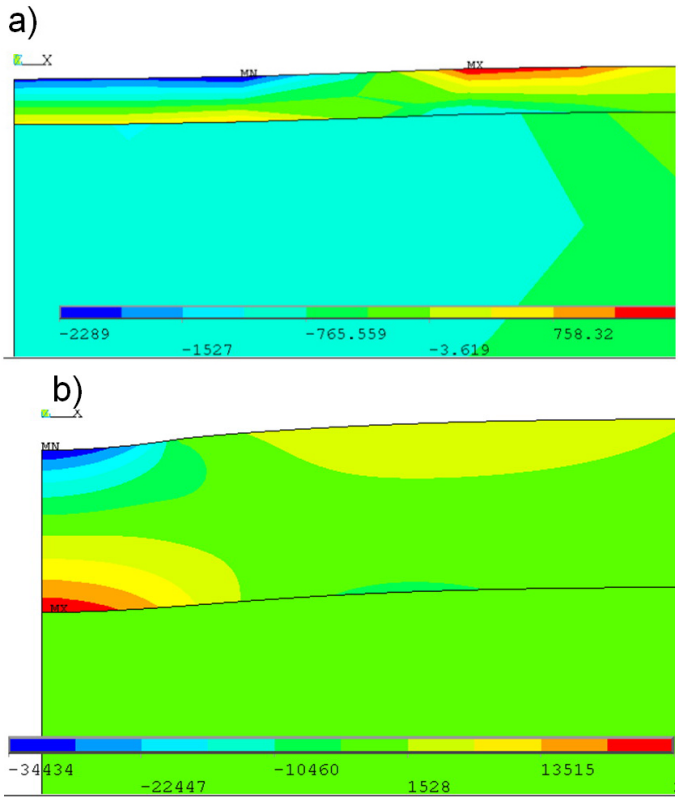

Fig. 7. Radial stress distribution in: a) thin t/R_i = 0,005, b) thick t/R_i = 0,25 coatings

The maximum of the tensile stresses is just outside the contact area on the surface of the thin coating. In the coating-substrate interface, the highest stress is in the indenter symmetry axis, but its level is lower than in the surface. For thick coatings the maximum stress is initially on the coating surface, like in the case of thin coatings. However, with the load increase, maximum stress concentration moves to the interface with the relative penetration depth $h_{max}/t > 0.03$ (Fig. 8).

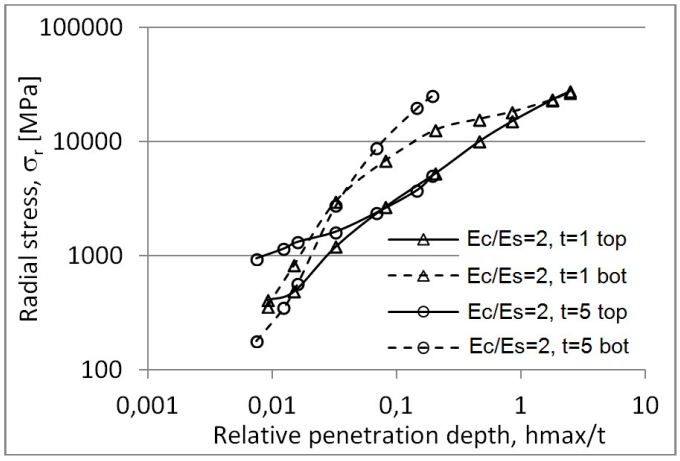

Fig. 8. Maximal radial stress on the top (top) and in the coating substrate interface (bot) for coatings two times stiffer than substrate E_c/E_s = 2 with thickness t = 1 and 5 µm, during spherical indentation with indenter tip radius R_i = 20 µm

FEM modelling results show that this deformation corresponds to the moment when the radius of the yielded zone r_{pl} in the substrate is about 2 times greater than the radius of the contact area a_c. Therefore, the range of substrate plastic deformation seems to be crucial for areas subjected to fracture. For thick coatings, the maxima of the tensile stresses in the coating surface appears at a large distance from the contact surface. This is confirmed by SEM observations where the circumferential cracks appear at even 3-5 times greater distance than the contact radius. Such cracks are presented in SEM images of a 2.4 µm thick TiN coating after indentation with R_i = 200 µm (t/R_i = 0.012), and R_i = 20 µm (t / R_i = 0.12) indenters – Figures 9a and 9b respectively.

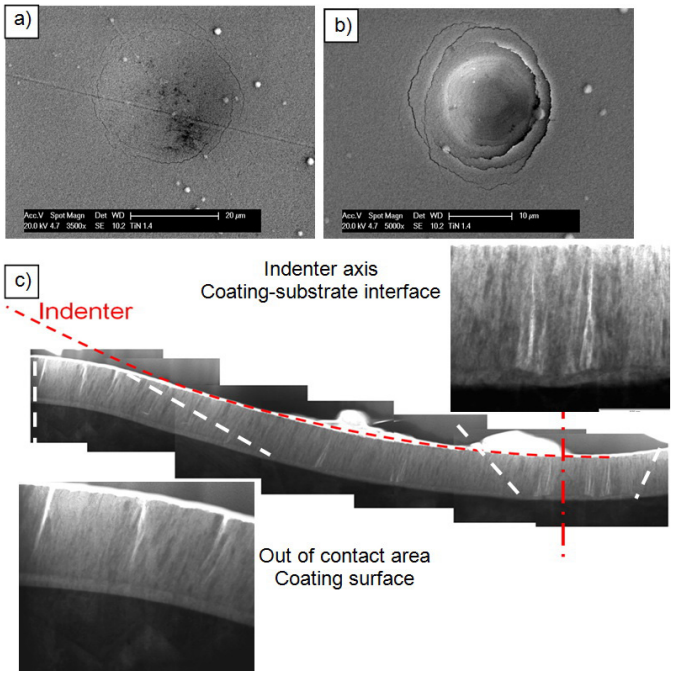

Fig. 9. Indents images after spherical indentation: a) SEM TiN = 2,4 R_i = 200 µm, b) SEM TiN = 2,4 R_i = 20 µm, c) TEM TiN = 1,4 R_i = 20 µm

Figure 9c shows the TEM image of the cross-section in the indent axis performed on a 1.4 µm TiN coated sample with clearly visible cracks in two characteristic areas – outside the contact zone in the surface and in the interface close to the symmetry axis. The changes in the stress concentration coefficient σ_R/p_m for coatings with varying thickness and the $E_C/E_S = 2$ ratio, which corresponds to many ceramic coatings on steel substrates, are presented in Figure 10. On the surface of the coatings, at low deformation, the coefficient σ_R/p_m is in the range 0.14-0.2. Load increase leads to a significant stress concentration in the surface (Fig. 10a) and in the interface (Fig. 10b).

For both these areas, σ_R/p_m rises with coating thickness. For the thinnest coating $t/R_i = 0.05$ ($t = 1$ µm, $R_i = 20$ µm), within the analysed load range, tensile stress at the surface can be up to five times higher than the mean pressure in the contact zone. Meanwhile for a thicker coating $t/R_i = 0.25$ ($t = 5$ µm, $R_i = 20$ µm), σ_R/p_m grows only up to 0.6. The same phenomena was found for stress concentration in the coating-substrate interface where σ_R/p_m reaches 5 and 1.5 for $t/R_i = 0.05$ and 0.25 respectively. In Figure 10, the dashed curves correspond to the same loads 50, 200, 500 and 1000 mN. For example, a 500 mN load induces the relative penetration depth $h_{max}/t = 1.2$ and 0.2 for the thinnest

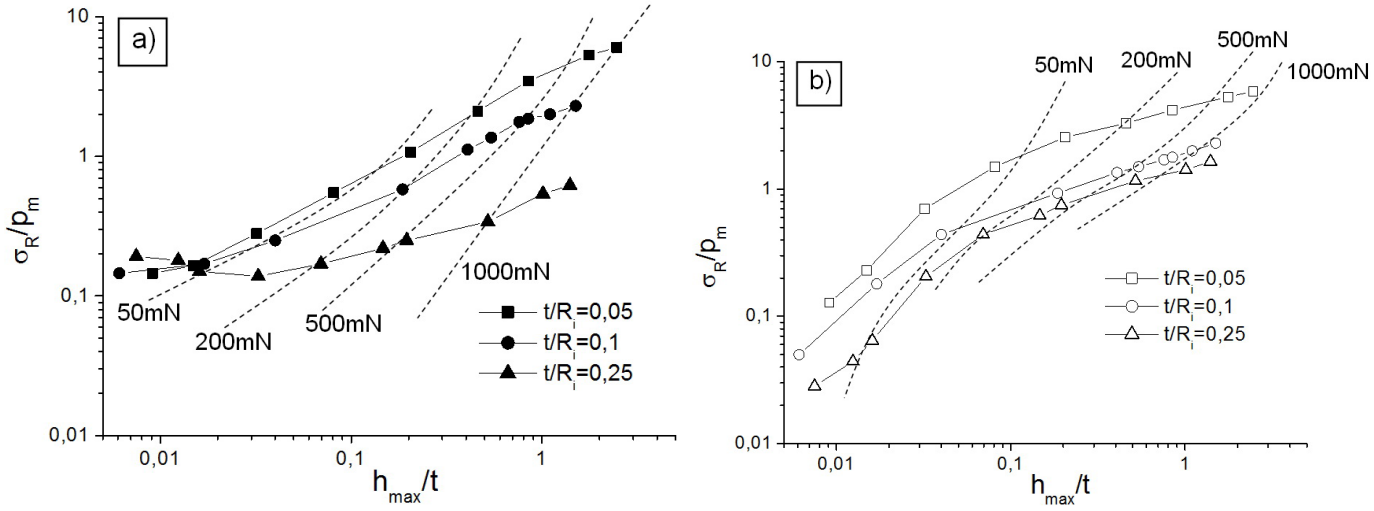

Fig. 10. Changes of the ratio of maximum radial stress to contact pressure σ_R/p_m as a function of relative penetration depth h_{max}/t for modulus ratio $E_c/E_s = 1, 2, 3$ and relative thickness range $t/R_i = 0.05$-0.25 in: a) coating surface, b) coating-substrate interface

and thickest coatings, while the stress concentration coefficient reaches 4 and 0.25 respectively. Although the stress concentration for thicker coatings is lower the radial stress, σ_R could be higher than in thinner ones due to the substantially higher pressure p_m in the contact zone to which they are referenced. Previous studies presented in [27] allowed the mathematical relation binding the stress concentration coefficient $C = \sigma_R/p_m$ with the relative penetration depth h_{max}/t on the surface (C_{Top}) and interface (C_{Bott}) to be determined:

$$C_{Top} = 0{,}14 + \left[\ln\left(\frac{t}{R_i}\right) + 1{,}15\right] \cdot \left[0{,}37 \cdot \left(\frac{h_{max}}{t}\right)^2 - 2 \cdot \frac{h_{max}}{t}\right] \cdot \left(\frac{E_c}{E_s}\right)^{\frac{1}{3}}$$

$$C_{Bott} = 0{,}13 + \left(\frac{E_c}{E_s}\right)^{0{,}47} \cdot \left(\frac{t}{R_i}\right)^{-\frac{2}{3}} \cdot \ln\left(\frac{h_{max}}{t}\right) + 0{,}4 \cdot \left(\frac{E_c}{E_s}\right)^{0{,}55} \cdot \left(\frac{t}{R_i}\right)^{-\frac{2}{3}} \quad (6)$$

4. Indentation results

Indentation tests using different tip radius spherical indenters with the algorithm shown in Figure 11 allow the calculation of the mean pressure changes in the contact zone.

Figure 11a shows the indentation curves of 1 and 5.2 µm thick CrN coatings obtained using a 10 µm indenter radius. The penetration depth of the indenter at the 200 mN load decreases from 1470 to 520 nm with increasing coating thickness from 1 to 5.2 µm. Subsequent curves for the larger indenter radii $R_i = 20$, 50 and 200 µm are presented in Figures 12a, 13a and 14a, respectively.

Comparing consecutive figures, the declining influence of the coating thickness (ratio t/R_i) on the deformation of the whole system is clearly visible. The penetration depth ratio values $P_d(t = 1\ \text{ρm})/P_d(t = 5.2\ \text{ρm})$ at 200 mN are 2.65, 1.57 and 1.35 for $R_i = 20$, 50 and 200 µm indenters, while for the smallest radius $R_i = 10$ µm this parameter is 2.82. Hence, one can conclude that the smaller the relative coating thickness, the lower the impact of the coating on the system deformation. The stress-strain curves calculated from the presented indentation curves on the following figures are shown in Figures 11b, 12b, 13b and 14b. The significant effect of the t/R_i ratio on the mean pressure p_m in the contact zone is presented in Fig. 11b where p_m reaches 3.5 and 7.3 GPa for $t/R_i = 0.1$ and 0.52 respectively (the results for all indenters are summarized in Table 1). For both coatings, pressure initially rises linearly up to the strain $\varepsilon = 0.02$-0.05. The systems are elastically deformed, which was confirmed by the results of tests carried out with a smaller load when loading and unloading

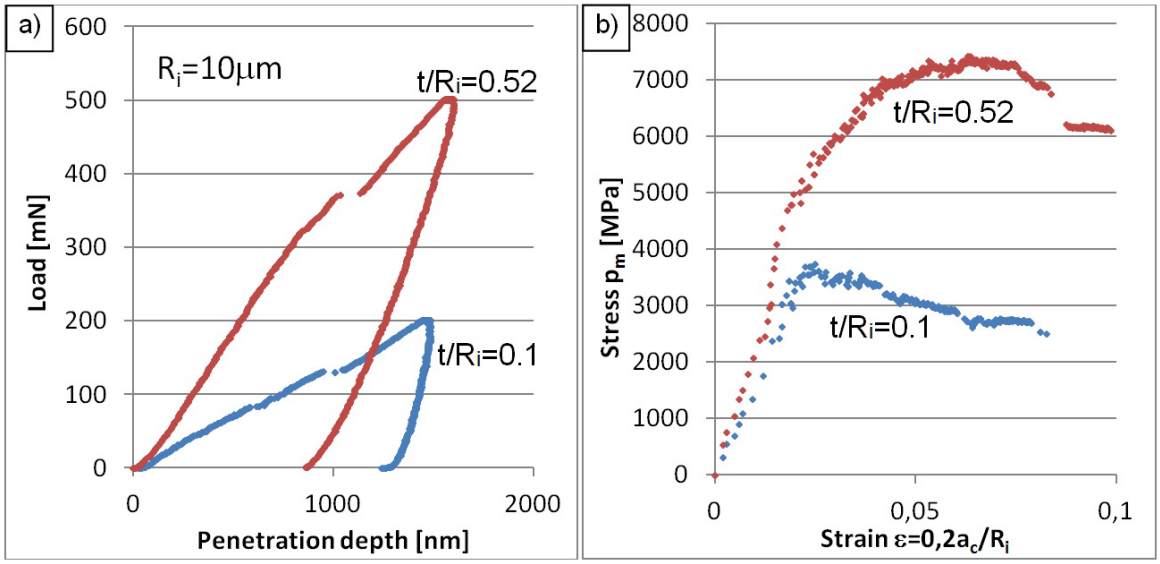

Fig. 11. Results of spherical indentation R_i = 10 μm of CrN coatings: a) indentation curves, b) stress – strain curves

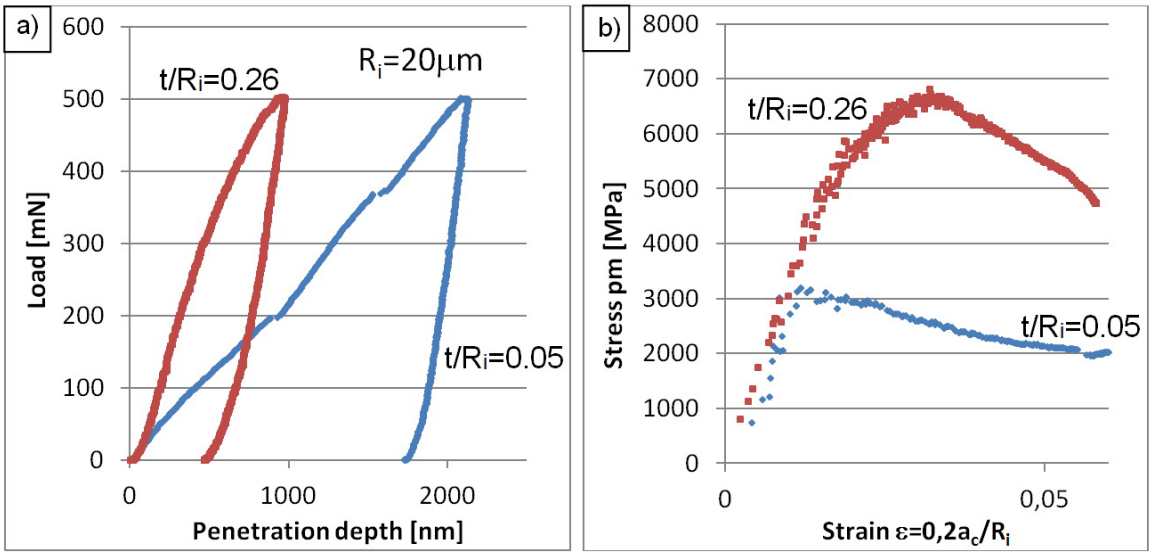

Fig. 12. Results of spherical indentation R_i = 20 μm of CrN coatings: a) indentation curves, b) stress-strain curves

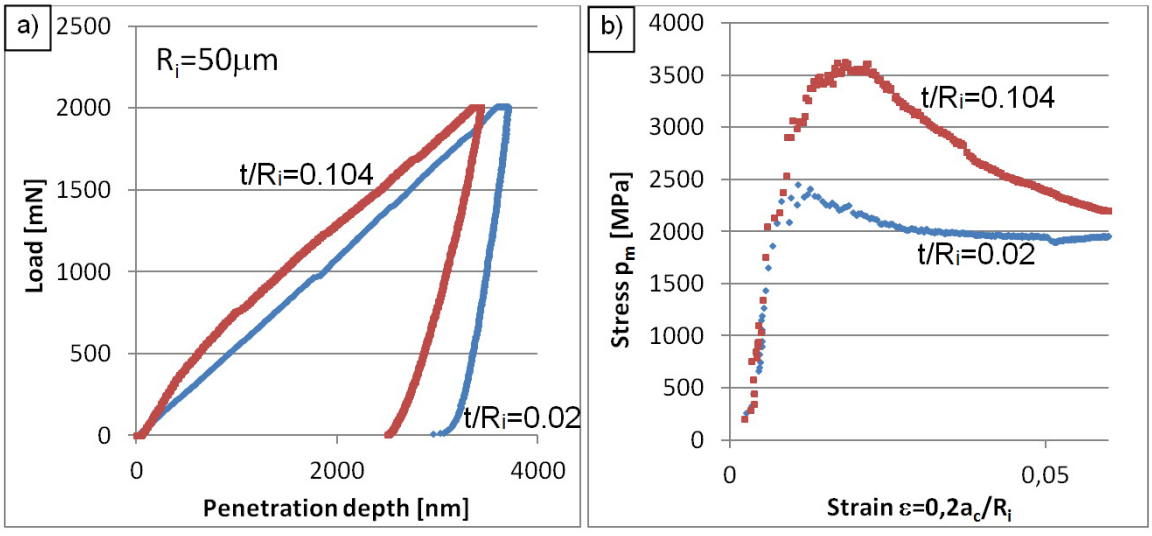

Fig. 13. Results of spherical indentation R_i = 50 μm of CrN coatings: a) indentation curves, b) stress-strain curves

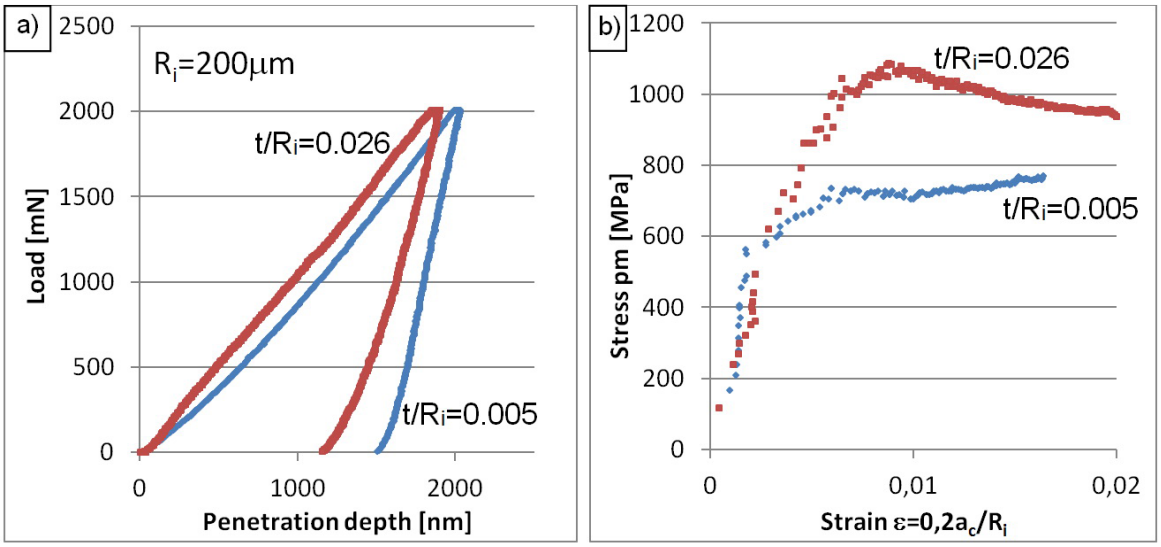

Fig. 14. Results of spherical indentation R_i = 200 µm of CrN coatings: a) indentation curves, b) stress-strain curves

curve overlaps and indents were not found after the test. Further load increase leads to substrate yield, which facilitates the easier deformation of the systems. This plastic deformation occurs at a lower load for a thinner coating, hence the stress-strain curve reaches its maximum at a lower pressure. For a thicker coating, the $\sigma - \varepsilon$ curve changes its slope at 5 GPa pressure, which may indicate the initial development of a plastically deformed zone. When the plastic deformation is highly extended, the substrate does not provide required support for the coating, and pressure starts to diminish as for the thin coating. The larger maximum pressure in the contact zone for thicker coatings is the result of its high stiffness and low contact area. For the R_i = 20 µm indenter radius, the mean pressure in the contact zone is smaller and reaches 3.1 and 6.7 GPa for 1 and 5.2 µm coating thickness, respectively (Fig. 12b). A further increase in indenter radius reduces the pressure to 2.7 and 5.2 GPa for R_i = 50 µm and 1 and 1.4 for R_i = 200 µm on the surface of the thinner and thicker coatings, respectively.

Large deformations of coating-substrate systems result in the tensile stress concentration on the surface of the coating and its fracture, which is evident on the indentation curves as a pop-in (sudden rise of penetration depth). The formation of the first circumferential cracks was observed at the F_{Fr} = 100 mN load for a 1 µm coating while for the thicker one t = 5.2 µm at 350 mN (Fig. 12a). The summary of relative critical loads leads to the coating fracture F_{Fr}/R_i^2, the corresponding relative penetration depth P_d/t, for all contact geometries and coating thickness are summarized in Table 1 and in Figure 15. The relative values of the apparent fracture toughness $Kc' \cdot R_i/t^{1/2}$ (onset of coating fracture, not the material parameter of coating), calculated as the integral of the stress-strain curve until the first crack, are also given in Table 1.

TABLE 1

Summary of the indentation results

Coating material	t [µm]	R_i [µm]	t/R_i	$p_{m\text{-}max}$ [GPa]	F_{Fr}/R_i^2	P_d/t	$Kc' \cdot R_i/t^{1/2}$ [MPa·m$^{1/2}$]
CrN	1	10	0.1	3.5	1143	0.80	1.76
	5.2		0.52	7.3	2457	0.18	1.96
	1	20	0.05	3.1	456	0.82	2.18
	5.2		0.26	6.7	1163	0.15	1.64
	1	50	0.02	2.3	164	0.93	4.46
	5.2		0.104	3.5	516	0.29	2.29
	1	200	0.005	0.8	96	1.6	4.56
	5.2		0.026	1.1	113	0.35	2.95
TiN	0.7	20	0.035	2.7	225	0.5	1.84
	2.4		0.12	5.2	525	0.21	2.01
	0.7	200	0.0035	1.0	9	0.6	2.05
	2.4		0.012	1.4	22.5	0.37	2.11

The relative increase in the fracture load F_{Fr}/R_i^2 with rising relative film thickness t/R_i for CrN coatings is presented in Figure 15. However, it occurs for $t/R_i > 0.02$. The thinner coatings crack at a relatively constant load of F_{Fr}/R_i = 90-130 N/mm^2, which indicates that such coatings cannot improve the load bearing capacity of the surface. For thicker coatings, the parameter F_{Fr}/R_i^2 increases and reaches a value of about 2200-2400 N/mm^2 for $t/R_i = 0.52$. Within the range $0.02 < t/R_i < 0.52$ coatings crack under increasing load, due to the rising rigidity of the system and force necessary to reach the required deformation to its destruction. As derived from Figure 10, the increase in t/R_i results also in the reduction of stress concentration both on the surface of the coating as well as in the coating-substrate interface. The lower stress concentration on the coating surface is due to a smaller bending of the thicker coating, especially just outside the contact zone. On the other hand, more flexible thin coatings allow greater deformation to fracture, which proves higher values of the relative penetration depth P_d/t at the first crack event for a 1 μm coating than for 5.2 μm indented by the same diamond (Table 1). For very thick coatings of $t/R_i > 0.52$ the value of F_{Fr}/R_i^2 remains constant. These coatings with such a high relative thickness start to crack at penetration depths below 20% of its thickness, which indicates a small effect of the substrate on the deformation, hence the coating fracture is limited by fracture resistance as in the case of an infinitely thick coating. The application of very thick coatings from the mechanical point of view is aimless, furthermore thick coatings generally exhibit lower adhesion to the substrates. The changes in the relative fracture toughness $Kc' \cdot R_i/t^{1/2}$ within the range of the relative thickness t/R_i are shown in Figures 15, 16.

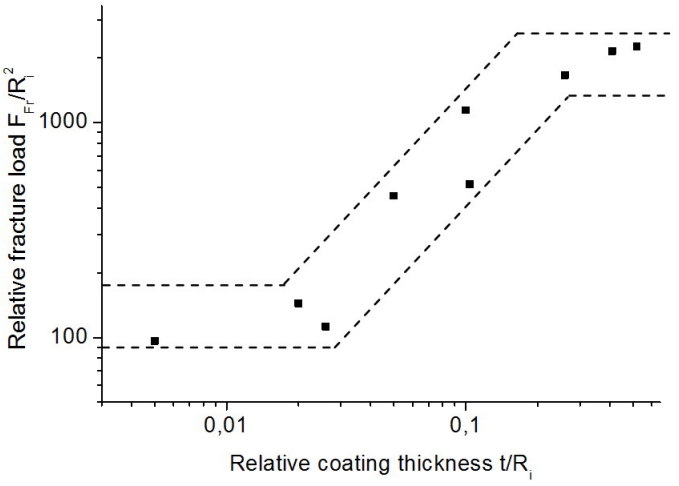

Fig. 15. Changes of relative fracture load vs. relative coating thickness of CrN coatings

Coatings thicker than $t/R_i > 0.2$ have this parameter at a relatively constant level of 1.6-2.3 MPa · m$^{1/2}$. Significantly higher values of $Kc' \cdot R_i/t^{1/2}$ = 4.5 MPa · m$^{1/2}$ were found for thin coatings $t/R_i < 0.2$, which confirms the higher fracture toughness of thin coatings presented in the literature [34].

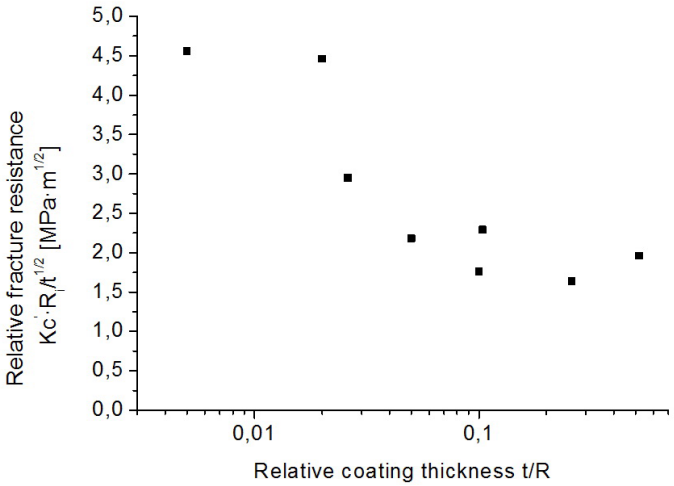

Fig. 16. Changes of relative fracture resistance vs. relative coating thickness of CrN coatings

5. Summary

The analysis of the deformation and fracture of coating-substrate systems given in the paper is a very important issue in the coatings tribology. The wear of such systems is substantially lower at loads below the critical level leading to coating fracture [12]. The presented studies allowed these critical loads for typical failure modes, like substrate yield and coating fracture by spherical indentation, to be determined. Tests performed with different radii of indenters enable the analysis of the load bearing capacity of coating-substrate systems at different states of deformation. By transformation of the typical load - the penetration depth curves into stress-strain curves, the analysis of mean stress changes in the contact area and coating fracture resistance is possible. The complete procedure for such analyses combined with the results of numerical experiments are presented in this paper. The results show the different character of the system deformation with thin and thick coatings. Coatings enhance the relative fracture load F_{Fr}/R_i^2 but only within $0.02 < t/R_i < 0.5$, which is clearly seen in the failure map of CrN coatings deposited on austenitic stainless steel substrates (Fig. 15). The thinner and thicker coatings have a constant value of the F_{Fr}/R_i^2 parameter. Despite the higher values of the stress concentration coefficient σ_R/p_m for thin coatings, the greater susceptibility of the whole system and lower mean pressure in the contact zone ensure its higher fracture toughness as presented in Figure 16. Systematic studies on the contact mechanics of coating-substrate systems and determination of their failure maps could be helpful in predicting the critical failure load during known contact geometry and optimizing coating thickness.

Acknowledgements

the author would like to thank Dr. habil. Juergen.M. Lackner from Joanneum Research Forschungsges. mbH, Institute for Surface Technologies and Photonics, Functional Surfaces, Niklasdorf, Austria for coatings deposition and Dr. habil. Lukasz Major from Polish Academy of Sciences, Institute of Metallurgy and Materials Sciences, Krakow, Poland for TEM analysis.

REFERENCES

[1] A. Erdemir, Tribology International **37**, 1005-1012 (2004).
[2] M. Kot, W.A. Rakowski, Ł. Major, R. Major, J. Morgiel, Surface and Coatings Technology **202**, 3501-3506 (2008).
[3] P. C. Yashar, W. D. Sproul, Vacuum **55**, 179-190 (1999).
[4] M. Kot, Ł. Major, K. Chronowska-Przywara, J.M. Lackner, W. Waldhauser, W. Rakowski, Materials and Design **56**, 981-989 (2014).
[5] A. Czyzniewski, Thin Solid Films **433**, 180-185 (2003).
[6] M. Kot, Ł. Major, J. Lackner, W. Rakowski, Journal of Balkan Tribological Association **18**, 92-105 (2012).
[7] J. Romero, J. Esteve, A. Lousa, Surface and Coatings Technology **188-189**, 338-343 (2004).
[8] J.M. Lackner, L. Major, M. Kot, Biulletin of Polish Academy of Sciences. Technical Sciences **59**/3, 343-355 (2011).
[9] M. Kot , Ł. Major, J. Lackner, Materials and Design **51**, 280-286 (2013).
[10] G. Gassner, J. Patscheider, P.H. Mayrhofer, S. Šturm, C. Scheu, C. Mitterer , Tribology Letters **27**, 97-104 (2007).
[11] H.C. Barshilia, B. Deepthi, A.S. Arun Prabhu, K.S. Rajam, Surface and Coatings Technology **201**, 329-337 (2006).
[12] M. Kot, W. Rakowski, J. Lackner, Ł. Major, Materials and Design **46**, 751-757 (2013).
[13] N. Dingremont, E. Bergmann, P. Collignon, H. Michel, Surface and Coatings Technology **72**, 3, 163-168 (1995).
[14] J.C.A Batista, C. Godoy, A. Matthews, Tribology International **35**, 6, 363-372 (2002).
[15] H. Hertz, Miscellaneous Papers, in: D.E. Jones, G.A. Schott (Eds.), Macmillan, London (1863).
[16] D. Tabor, Hardness of metals, Oxford: Clarendon Press (1951).
[17] Liu SB, A. Peyronnel, Q.J. Wang, L.M. Keer, Tribology Letters **18**, 303-314 (2005).
[18] A.C. Fischer-Cripps, Surface and Coatings Technology **200**, 4153-4165 (2006)
[19] Z. Jiang, F.X. Lu, W.Z. Tang, S.G. Wang, Y.M. Tong, T.B. Huang, J.M. Liu, Diamond and Related Materials **9**, 1734-1738 (2000).
[20] Z. Chen, B. Cotterell, W. Wang, Engineering Fracture Mechanics **69**, 597-603 (2002).
[21] S. Zhang, D. Sun, Y.Q. Fu, H. Du, Thin Solid Films **469-470**, 233-238 (2004).
[22] X. Li, B. Bhushan, Thin Solid Films 355-356, 330-336 (1999).
[23] J. Michler, E. Blank, Thin Solid Films **381**, 119-134 (2001).
[24] T. Pachler, R.M. Souza, A.P. Tschiptschin, Surface and Coatings Technology **202**, 1098-1102 (2007).
[25] X.C. Zhang, B.S. Xu, H.D. Wang, Y.X. Wu, Y. Jiang, Materials Design **28**, 47-54 (2007).
[26] M. Kot, Archives of Civil and Mechanical Engineering **12**, 464-470 (2012).
[27] M. Kot, J.M. Lackner, Ł. Major, W. Rakowski, Materials and Design **43**, 99-111 (2013).
[28] P. Wang, X. Wang, T. Xu, W. Liu, J. Zhang, Thin Solid Films **515**, 6899-6903 (2007).
[29] L. Zhang, H. Yang, X. Pang, K. Gao, A.A. Volinsky, Surface and Coatings Technology **224**, 120-125 (2013).
[30] ANSYS, Release 11.0 Documentation for ANSYS. ANSYS, Inc. (2007).
[31] J. Michler, E. Blank, Thin Solid Films **381**, 119-134 (2001).
[32] E. Weppelmann, M.V. Swain, Thin Solid Films **286**, 111-21 (1996).
[33] Z.H. Xie, R. Singh, A. Bendavid, P.J. Martin, P.R. Munroe, M. Hoffman, Thin Solid Films **515**, 3196-201 (2007).
[34] J. Chen, S.J. Bull, Thin Solid Films **494**, 1-7(2006).

Received: 20 April 2015.